

# QVD Sensors as Focal Plane Instruments for X-ray Timing Applications

Kent S. Wood<sup>\*</sup>, Armen M. Gulian<sup>#</sup>, and Paul S. Ray<sup>\*</sup>

<sup>\*</sup>Naval Research Laboratory, Washington, DC 20375

<sup>#</sup>Physics Art Frontiers/Naval Research Laboratory, Washington DC 20375

**Abstract.** “QVD” detectors are based on thermoelectric heat-to-voltage ( $Q \rightarrow V$ ) conversion and digital ( $V \rightarrow D$ ) readout. For spectroscopic applications, the theoretical performance limits are competitive with superconducting tunnel junction (STJ) detectors and transition edge sensor (TES) devices. We discuss theoretical and demonstrated timing performance of QVD detectors with different design architectures. Detectors with lanthanum-cerium hexaboride sensors can be very fast, up to 100 MHz/pixel counting rates. They can serve as focal plane detectors for X-ray timing, in situations where very large apertures are used to gather X-ray photons at high event rates. Practical implementation of thermoelectric (QVD) detectors requires cryogenic thermoelectric sensors with high figures of merit. There can be different solutions: thin films, bulk materials and “whiskers.” We are exploring all three design options and summarize progress in each area.

## 1. INTRODUCTION

The QVD detectors have an advantage of very high photon counting rates much higher than demonstrated by its major competitors, STJ and TES detectors (Fig. 1, left). At the same time there is no compromising in (theoretical) energy resolution or spectral resolving power (Fig. 1, right).

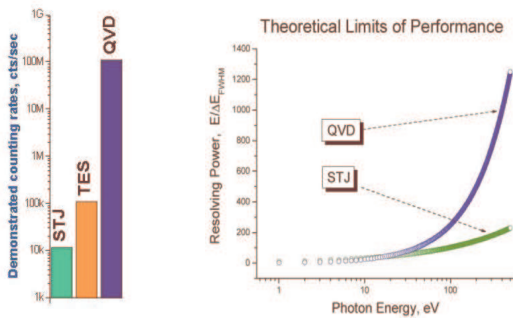


FIGURE 1. Comparison of detectors.

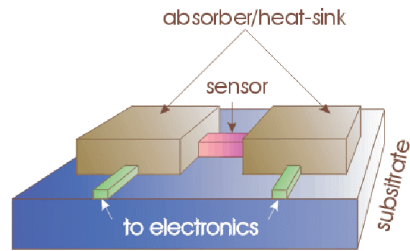
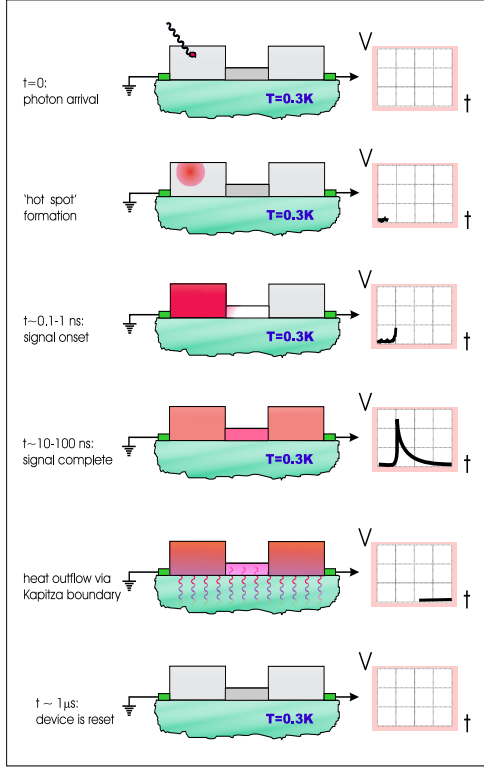


FIGURE 2. “Classical” design of QVD-detector, based on thermoelectric thin film sensor.

The QVD detector is based upon unavoidable thermoelectric effects as shown in Figs. 2 and 3. It is simple in design, and allows straightforward signal to noise modeling (see Section 2). It requires materials with high Seebeck coefficient ( $S = \delta V / \delta T$ ), which are known. We initially used Au(Fe) devices to validate the model. Higher  $S$  leads to devices with better performance.



**FIGURE 3.** Operational cycle of QVD detector

$\text{La}(\text{Ce})\text{B}_6$  has a high Seebeck coefficient in bulk; its film properties are being investigated. The operating temperature is  $\sim 400\text{mK}$ , comparatively high relative to TES devices. It is promising for very high speed (MHz counting rates vs. kHz in TES) applications.

## 2. QVD EXPECTED BEHAVIOR FROM FIRST PRINCIPLES

### 2.1. Signal To Noise Derivation

For the Johnson noise of the detector in Figure 2 we have:

$$V_{J.n.} = (4k_B TR\delta v)^{1/2}, \quad (1)$$

where  $R$  is the resistance of the sensor strip, and correspondingly,

$$\{<(\delta E_{J.n.})^2>\}^{1/2} = (2L_0/S)[(k_B T)(C_{\text{abs}} T)]^{1/2}, \quad (2)$$

where  $L_0$  is the Lorentz ratio:  $L_0 = (\pi^2/3)(k_B/e)^2 \sim$

$\sim 25 \text{ nW } \Omega/\text{K}^2$ , and  $C_{\text{abs}}$  is the absorber heat capacity. Equation (2) assumes that at sufficiently low temperatures the Wiedemann-Franz type behavior  $L = K/\sigma T$  is valid: the Lorenz Number,  $L \sim L_0$ . We confirmed experimentally that it is the case for  $\text{La}(\text{Ce})$  hexaborides. Another noise mechanism is the inter-pixel noise, for which

$$\{<(\delta E_{i.p.})^2>\}^{1/2} = 2 [(k_B T)(C_{\text{abs}} T)]^{1/2}. \quad (3)$$

Yet another noise source is driven by substrate-pixel heat conductance  $G$  with noise equivalent power:

$$\text{NEP} = 4k_B T^2 G. \quad (4)$$

Since the Kapitza time (this time is related to thermal resistance at the boundary metal-dielectric) is large:

$$\tau_K = r_0 C_{\text{abs}} / T^3 A_{\text{abs}} \gg \tau_{\text{signal}}, \quad (5)$$

where  $r_0 \sim 20 \text{ K}^4 \text{cm}^2/\text{W}$  is “universal” for metal-dielectric interfaces, and  $\tau_{\text{signal}} = C_{\text{abs}} R / (L_0 T)$ , the first two noise terms are dominant. Comparing this noise with the Seebeck voltage, i.e., the signal of our detector:

$$V(t) = \int S(T) \text{grad} T(t) dl = \int S dT = S \delta T(t), \quad (6)$$

we obtain its energy resolution in the form:

$$\Delta E_{\text{FWHM}} = 2.35 \{2k_B T^2 C_{\text{abs}} [1 + L_0/S^2]\}^{1/2}. \quad (7)$$

We can use these expressions to evaluate the key parameters of the QVD detectors.

## 2.2. Key Operational Parameters

### 2.2.1. Signal Duration (Timing)

Choosing  $C_{\text{abs}} \sim 10^{-15} \text{ J/K}$ , one can get  $\tau_{\text{signal}} \sim C_{\text{abs}} R / (L_0 T) \sim 10^{-8} \text{ sec}$  [at  $T \sim 0.5\text{K}$ ,  $R \sim 0.1\Omega$ ]. Thus the time resolution can be as fast as  $10^{-8} \text{ sec}$ . It can be faster for softer photons since  $C_{\text{abs}}$  can be chosen smaller.

### 2.2.2. Counting Rate

Counting rate is determined by the longest (“Kapitza”) time  $\tau_K = r_0 C_{\text{abs}} / T^3 A_{\text{abs}} \sim 10^{-7} \text{ sec}$  at  $A_{\text{abs}}$  (absorber-substrate interface)  $\sim 200 \mu\text{m}^2$  at lateral pixel dimensions  $\sim 15 \mu\text{m}$ . This is essentially the dead time associated with the fifth stage in Fig. 3, during

which the system recovers. Thus one can expect  $\sim 10^6 - 10^7$  cts/sec/pixel for thin film sensor QVD devices.

### 2.2.3. Quantum Efficiency

For QVD detectors the quantum efficiency equals absorption efficiency and depends on the absorber material and thickness; for a bismuth absorber:  $C_V(\text{Bi}) \sim 4 \times 10^{-6} \text{ J/cm}^3 \cdot \text{K}$  at  $T_{\text{op}} \sim 0.5 \text{ K}$ , and at thickness  $d = 1.5 \mu\text{m}$   $C_{\text{abs}} \sim C_V(\text{Bi}) \times V (\sim 300 \mu\text{m}^3) \sim 10^{-15} \text{ J/K}$  and one can get efficiency about 50% at 6 keV events (higher at smaller energies, see Figure 4).

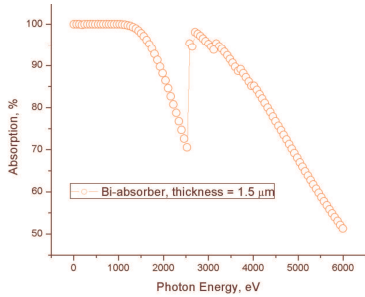


FIGURE 4. Absorption efficiency in Bi film

### 2.2.4. Energy Resolution

Energy resolution [in eV] is given by Eq. 7. At  $C_{\text{abs}} \sim 10^{-15} \text{ J/K}$  and  $T \sim 0.5 \text{ K}$ , we get  $\Delta E_{\text{FWHM}} \sim 2 \text{ eV}$ . This value of  $C_{\text{abs}}$  is appropriate for 6 keV photons. For UV photons  $C_{\text{abs}}$  could be chosen smaller by orders of magnitude and yield higher resolution values (0.1 eV and better).

## 3. DEVICES AND DEMONSTRATIONS

During the last few years several generations of prototype detectors were fabricated. The following schemes (Figs.5,6) were mainly used for their testing.

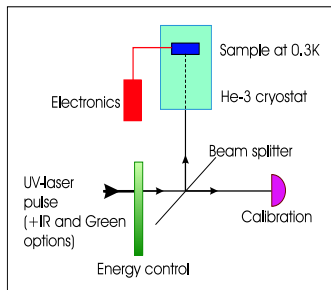


FIGURE 5. QVD testing scheme.

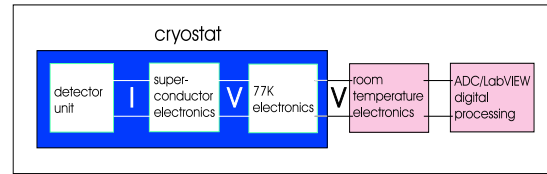


FIGURE 6. Prototype detector testing electronics.

A laser source generated enveloped pulse trains with the sub-ns duration of pulses and 20 ns length of the envelope at FWHM.

### 3.1. First Devices With Au-Fe Sensors

The output of the first detectors which reached 500eV resolution at  $\sim 6 \text{ keV}$  energy input is shown in Fig. 7, and the device – in Fig. 8.

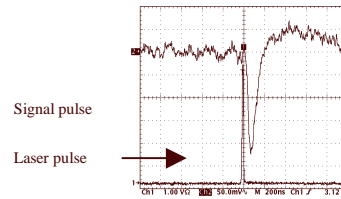


FIGURE 7. Output of Au-Fe sensor devices.

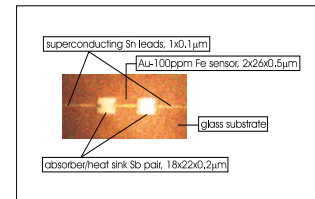


FIGURE 8. Au-Fe sensor devices.

These devices had  $S \sim 0.3 \mu\text{V/K}$  and  $R \sim 1-10 \Omega$ . The overall agreement with the theory is very good.

### 3.2. Detection Experiments With Hexaboride Crystals

The figure of merit  $ZT = S^2/L$  of hexaboride crystals can be  $>0.1$  at cryogenic temperatures ( $T < 4 \text{ K}$ ). This means that the energy resolution will be much higher than with Au-Fe devices. We have not yet been able to manufacture thin film hexaboride crystals, though the work is in progress in that direction. Meanwhile, we were able to make some experiments with single-crystalline QVD sensor designs. Two prototype embodiments were analyzed: one with flat crystal sensor and one with whisker-type sensor geometry.

### 3.2.1. Flat Crystal Design

The devices in this design (see Figs. 9 - 11) can operate even faster than thin-film devices (no Kapitza resistance), though the modeling of S/N for deriving the energy resolution is not yet done: the suppression of substrate noise may become an issue.

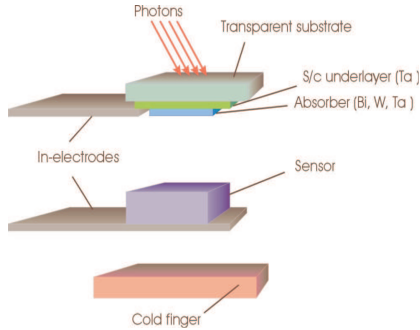


**FIGURE 9.** Exploded view of the flat sensor QVD.

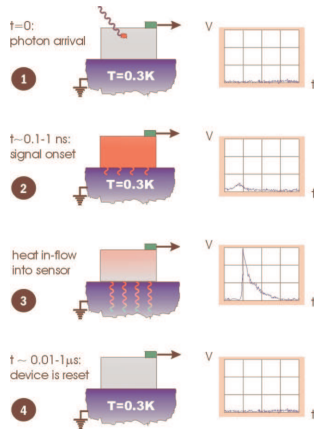


**FIGURE 10.** Operational cycle of flat sensor QVD.

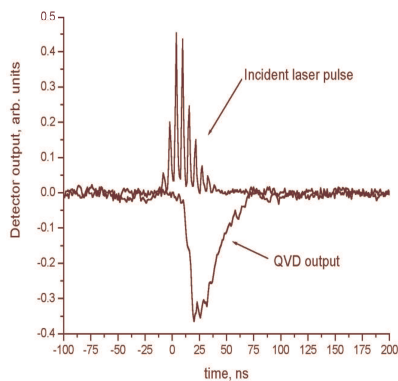


**FIGURE 11.** Time resolution of flat sensor QVD.

As this figure demonstrates, the counting rate can be close to  $10^8$  cts/sec!

### 3.2.2. Whisker Sensor Design

Growth of  $\text{LaB}_6$  crystals is possible in a whisker form, and it is possible to do that in a form of regular arrays. Keeping that in mind, we prototyped a “whisker” option of the QVD shown in Fig. 12.



**FIGURE 12.** (left) Single-crystalline splinter glued in kapton serves as a whisker-like sensor; (center) array of Bi-absorbers ( $\phi=25 \mu\text{m}$ ; thickness  $1.4 \mu\text{m}$ ); deposited on plastic substrate thinned with a half-drilled hole (shown upside-down); (right) top-view of the detector: assembly aligns absorber, whisker.

Figure 13 demonstrates the output of this prototype detector, which proves the viability of whisker design.

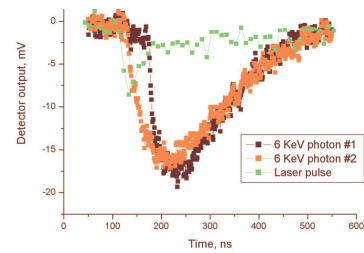


**FIGURE 13.** Output of the whisker-sensor QVD.

## 4. CONCLUSIONS

We have demonstrated the high thermoelectric figures of merit of hexaboride crystals, demonstrated that they are suitable for reaching the ultimate performance of QVD detectors. These detectors can have very high timing resolution (down to few nanoseconds) and high counting rates  $10^7$ - $10^8$  cts/sec per pixel. Each pixel event can in principle be tagged with energy resolution as high as  $\Delta E_{\text{FWHM}} \sim 1$ - $10$  eV at 6 keV.

## ACKNOWLEDGMENTS

This work is supported in part by DARPA, ONR, and NASA. We are grateful to D. Van Vechten, G. Fritz, B. Philips, A. Kuzanyan, V. Nikoghosyan, V. Vartanyan, S. Harutyunyan, G. Badalyan, K. Winzer, S. Kunii, C. Mitterer, M. Carllson, V. Gurin, N. Korsukova, V. Novikov, H.-D. Wu, C. Boyer, G. Holland, S. Bounnak, and F. Golf.